Max H2 DR

Maximise H2 Enrichment in Direct Reduction Shaft Furnaces

Pellet reduction kinetic model adapted to multiparticle reactor models

Deliverable D1.4 by WP1. Partners: UL, BFI, RUB M27

Antoine Marsigny, Olivier Mirgaux, Fabrice Patisson (UL)

Thorsten Hauck, Yalcin Kaymak, Thomas Piontek, Kersten Marx (BFI)

Klidi Qyteti, Enric Illana, Victor Scherer (RUB)

February 2025

This project has received funding from the European Union under grant agreement NUMBER — 101058429 — MaxH2DR

Table of contents

List of Figures

List of Tables

1. Introduction

The present Deliverable reports the work carried out by UL, BFI and RUB within the framework of Task 1.4 “Implementation of new kinetic sub-models into DR shaft process” of work package 1 “New fundamental knowledge and sub-models” for the first 27 months of the MaxH2DR project.

A significant modelling effort is planned for the project: different types of models (Finite Volume Model, Finite Element Model, Discrete Element Model) for the simulation of a H_2-enriched DR (Direct Reduction) shaft reactor, as well as systems models based on global mass and heat balances for DR plant simulation. These models need to rely on an accurate description of the iron ore reduction reaction kinetics. This description will be based on kinetic sub-models simulating the transformation of iron ore grains and pellets, the sub-models being implemented in the reactor and plant models.

Task 1.3 has been devoted to the development of these kinetic sub-models. In addition to being necessary to the reactor and plant models, the kinetic models are also useful in determining the proper intrinsic kinetic parameters from a comparison between the measured (Task 1.1) and calculated (Task 1.3) data.

The present report describes the adaptation of the pellet reduction kinetic models for the application in the multiparticle reactor model along with the preliminary results obtained so far.

The mechanical properties of iron-ore pellets change during the reduction process, transforming from relatively hard spherical objects into sintered sponge iron products. This transformation includes a temporary "sticky" phase that affects both mechanical movement and gas flow and must be considered in coupled simulations. Understanding how these material properties vary in the context of larger particles is essential for extrapolating reliable data and comprehending the implications of such changes on the broader material flow process.

Shear-cell experiments in Task 1.2 address the quantitative parameters related to friction and sintering. Since the actual ore pellets were not available at the start of the project, initial simulations have been conducted using 6 mm and 10 mm wooden spheres in a shear cell configuration provided by the University of Salerno (UNISA). These preliminary simulations at cold conditions aim to replicate the corresponding shear cell experiments, in which UNISA measured the normal force, shear force, and pellet displacement. These simulations are the first validation step before evaluating the "hot" experiments with DRI pellets planned at UNISA. This set of simulations aims to evaluate the extent to which crucial parameters such as stiffness, friction and cohesion coefficients, can be derived from shear cell experiments.

2. Adaptation and Integration of sub-models

2.1. Single Pellet Kinetic Model

The **S**ingle **P**ellet **K**inetic **M**odel (SPKM) built by UL describes the reduction and the carbon deposition for a single hematite pellet through eight reactions (six for the reduction, two for the carbon deposition). It represents the pellet structure based on a grain model modified with the law of additive reaction times and is initially designed to work in isothermal and constant gas composition conditions. The complete description of the model is available in Deliverable D1.3.

This new stand-alone model can be used with different targets:

- simulate the behavior of one pellet under constant external conditions (like a pellet undergoing a reduction experiment in a thermobalance) or variable external conditions (like a pellet descending in a DR shaft furnace),
- determine kinetic constants from curve fitting between calculated and measured data,
- be integrated in a multiparticle reactor model.

The temperature dependency of the hydrogen reduction of an iron ore pellet is qualitatively described by the model (see Figure 1). The model gives quite satisfactory results for the simulation of a pellet reduced in a thermobalance between 700 and 900°C, which is the usual range of temperature encountered in DR shaft furnaces. It is accurate at describing the reduction with both 100% hydrogen and helium-diluted hydrogen gas compositions. These results and other are available in D1.3.; they have been validated against reduction experiments from T1.1.

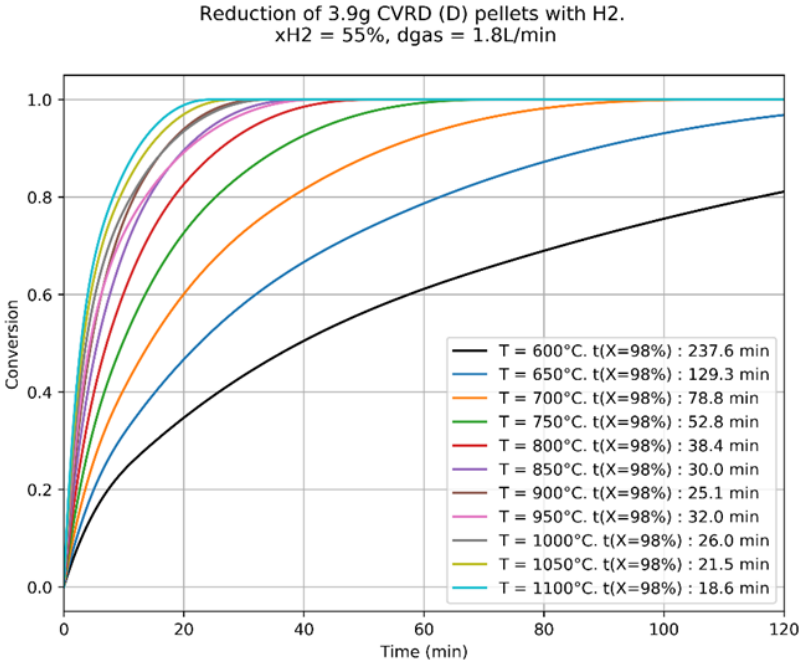

Figure 1: Simulated reduction of CVRD (D) pellets in the (600-1100) °C temperature range. The global T dependency and the kinetic slowdown at 950°C can already be distinguished here.

The SPKM has been numerically implemented in an in-house Python code in T1.3. The latter has been made available to the other partners of MaxH2DR who refined the kinetic parameters through mathematical optimization (curve fitting between calculated and measured data). The models were then implemented in the DR shaft models of the MaxH2DR consortium. Details are given in the following chapters.

Optimization of the kinetic triplets

Due to the extreme intricacy in describing the reduction mechanisms at the molecular scale, regular generic Arrhenius laws are used to determine the reaction rate of the reduction sub-reactions.

$$k_i = k_{0,i} \exp\left(-\frac{Ea_i}{RT}\right) \quad \text{(i = 1,2,3)}$$

The kinetic triplets $\left(k_{0,i}\ ,\ Ea_i\right)$ are to be determined experimentally by mathematical fitting.

Due to the superposition of the reactions, the influence of each kinetic parameter is hard to quantify, and a descent algorithm is difficult to implement. To mitigate this issue, a less regular optimization algorithm is used based on pattern search. With given initials values for each kinetic triplet, optimization is achieved by successive trials in which the area of random search for the parameters progressively shrinks.

The kinetic triplets are determined by mathematical fitting of simulated curves against experimental reduction curves provided by TSE Ijmuiden. In their setup, called a batch furnace, a bed of 500 g of pellets is reduced by a gas flow containing 10 Nl.min^{-1} of hydrogen. In the case of batch reduction, a non-negligible amount of hydrogen is consumed during the reduction, which leads to H_2 depletion in the furnace. This phenomenon leads to much slower reduction and is not considered in the SPKM, which considers a static gas atmosphere. This implies the need for an adaption of the model to this situation.

To this end, an updated version of the SPKM was elaborated. It simulates the reduction of a pellet (or batch of pellets) in dynamic gas conditions, namely with variations in the H_2/H_2O ratio in the gas due to the reduction. The code was updated by implementing a simple 1D plug flow CFD Framework in which both furnace and pellets are discretized. Benchmark against corresponding implementations from BFI and RUB was realized, and the results are in clear accordance (see e.g. Figure 22).

The fitting of kinetic triplets was achieved in the 600-900°C temperature range with a mean pellet diameter of 12 mm. Results are given in Figure 2. A comparison with literature shows that optimized values are in the usual range of activation energies for these operating conditions. The kinetic parameters thus obtained are now the ones used by all partners in the MaxH2DR project.

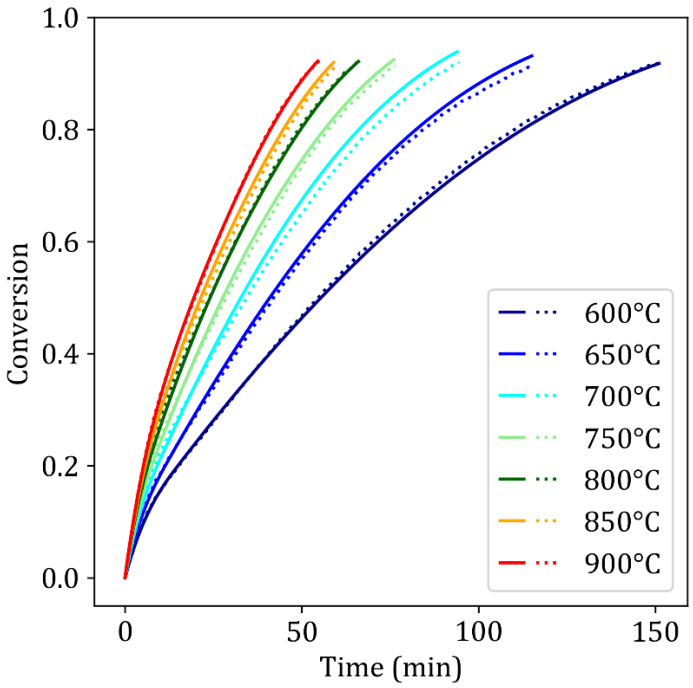

Figure 2: Optimized results of the simulation of the reduction of 12mm pellets by an 18 Nl.min^{-1} gas flow of 55% H_2 and 45% N_2 in the TSE batch furnace. Simulated curves are solid lines and experimental curves are dotted lines.

2.2. Shear cell simulations

UNISA carried out shear tests with beech wooden spheres. In these Schulze tests, two series of tests were carried out. In the first one, the particle diameter was approximately ten millimeters while in the second one the diameter was six millimeters. In a series of tests, three different load levels of 15 N, 25 N and 50 N were recorded. The aim of this work is to simulate these Schulze tests with the same number of particles and load levels using the DEM code from the Chair of Energy Systems and Energy Process Engineering at the Ruhr University Bochum (LEAT).

With the shear cell simulation, theoretically approximate parameters can be determined by comparing them with experiments. There are few sources [1,2] in which wood was simulated in the form of spheres. Pellets or fibers are usually simulated as these often appear in real applications. Due to their fiber structure, wooden particles have anisotropic properties, and they influence the behavior of an individual particle. For example, wood is easier to deform along the grain direction than perpendicular to it; this affects the deformation during the collision as well as the fracture behavior [3]. For simplicity, this is not taken into account in the simulation.

Contact model

As the particle system to be simulated has a high density, collision between spheres must be modeled. The soft sphere approach is a simulation method for bulk solid dynamics that has been used early on. It was published in 1979 by Peter A. Cundall and Otto DL Strack [4] and is the basis for many extensions and further developments of today's DEM modeling approaches. In fact, it is the most widespread and diverse approach [5]. The movements of the particles are described by integrating Newton's equation of motion and the contacts of the particles are modeled by forces at the atomic and molecular or macroscopic levels. Due to this higher level of detail and the more extensive contact modeling, this approach leads to more realistic simulations.

The model used for computing the forces is a linear spring-dashpot. The model parameters (tangential and normal spring stiffness as well as the tangential and normal damping coefficients) can be specified directly or calculated. In this work, the alternative of calculating the mass-related model parameters was chosen. For this purpose, the restitution coefficient, the ratio of tangential to normal spring stiffness and the contact time are required as input variables for the linear spring-dashpot model [6]. In addition, the coefficient of rolling friction is specified so that the moments caused by the rolling of the particles are not too high. The value of these parameters is given in the table below:

Table 1: Parameters used for the interaction between wooden pellets and the shear cell surface for the two simulations

Parameter	Value (particle-particle)	Value (particle-surface)
Rolling friction	0.002	0.002
Sliding friction	0.3	0.6
Coefficient of restitution	0.3	0.7
Collision time	0.001	0.001
Particle density	720 kg/m³	

Simulation Setup

The components of the shear cell (the lid and the annular cell) are complex geometries based on 3D models that were constructed according to the dimensions of the actual shear cell. These 3D models employ a network of polygons (in this case triangles). Figure 3 shows the 3D model of the lid of the shear cell used.

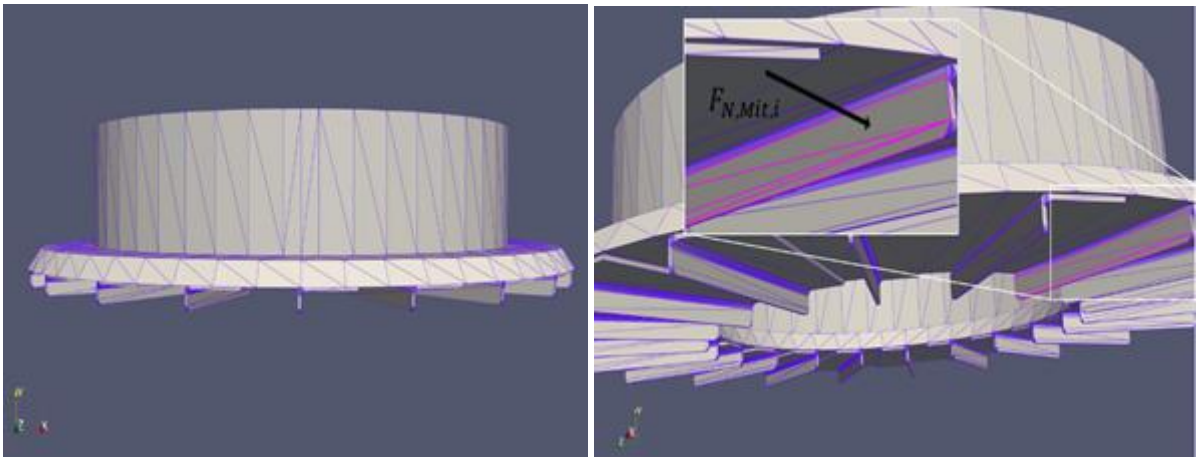

Figure 3: The 3D model of the lid with representation of the polygon mesh and the normal force acting on it on the right.

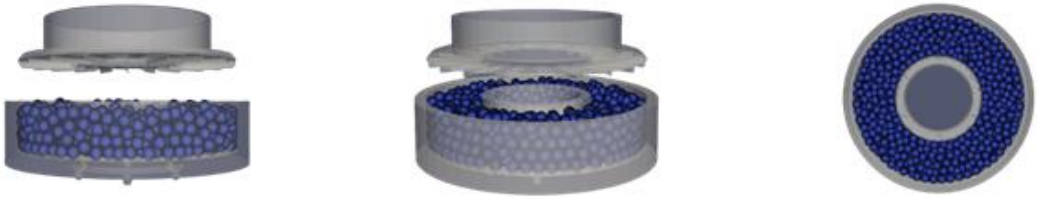

Figure 4: Shear Cell simulation setup.

The lid is lowered onto the spheres until the desired normal force is exerted upon them. Once positioned, the normal force remains constant. Adjusting the vertical position of the lid allows for the setting and maintenance of all normal force levels required for the shear test. This is illustrated on Figure 4, where the results from the experiments from UNISA, where the normal force is measured by a sensor placed on the lid, are compared with the simulations from RUB, where the normal force is calculated from the sphere-lid mechanical interactions. Particularly, the normal force exerted from the particles on the lid during a time step is determined by adding up the forces acting on each of the polygons of the lid in the perpendicular direction.

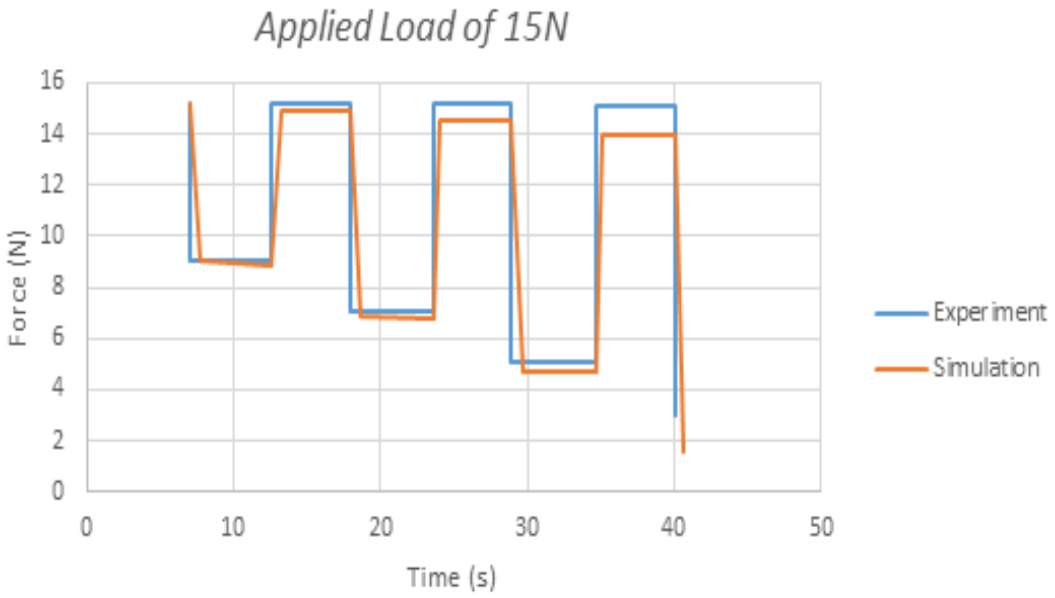

Figure 5: Normal force curves from simulations and from the experiments for the consolidation load of 15 N.

Figure 5 shows the comparison of normal force curves obtained from the simulations (red line) and the experiments (blue line) for the scenario without bottom ring rotation. This trend of close agreement between simulations and experiments holds true for other force levels as well, as illustrated in Figure 6.

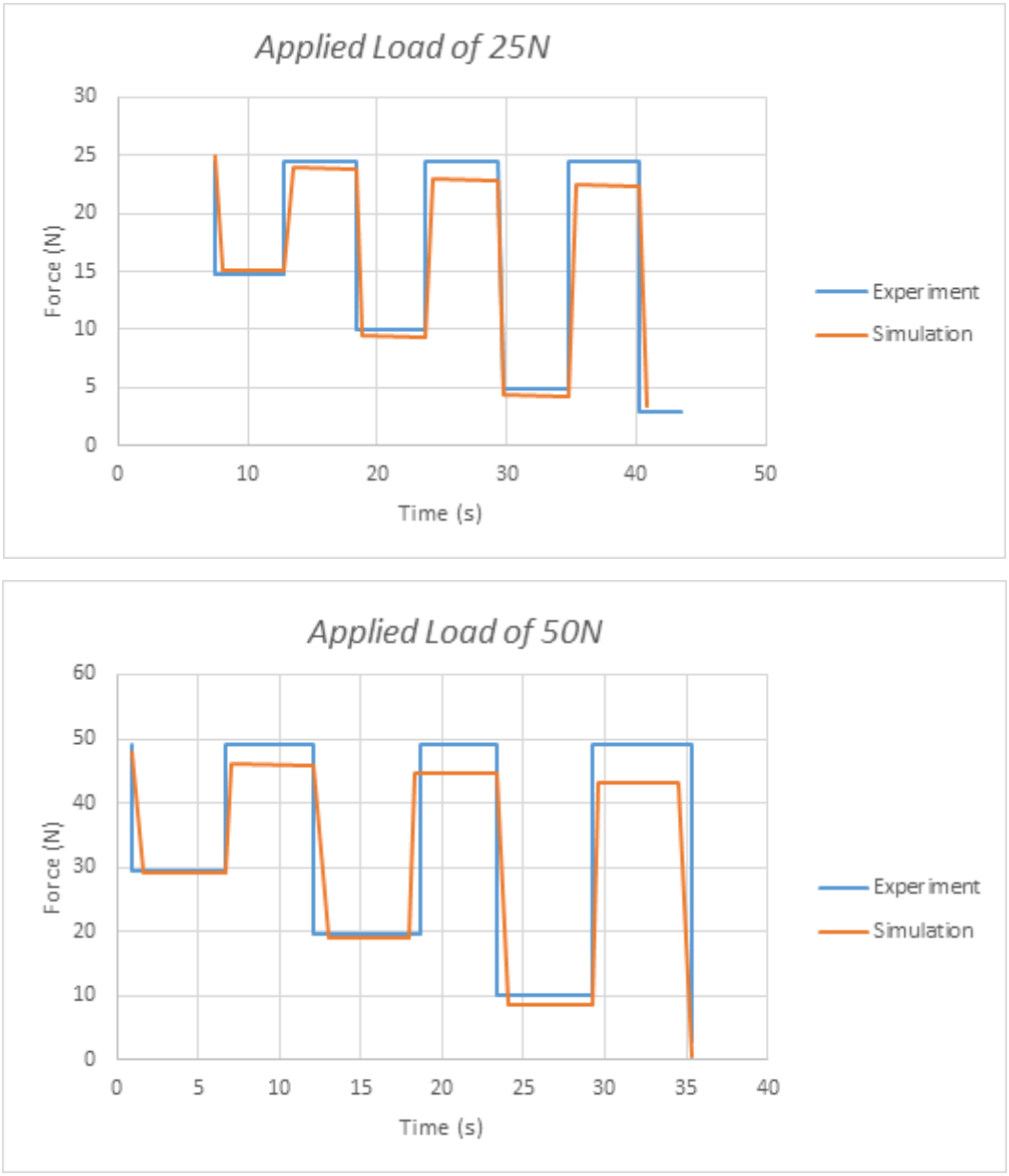

Figure 6: Normal force curves from simulations and from the experiments for consolidation loads of 25 N and 50 N

Additional simulations were conducted to further explore the influence of particle size on shearing behavior. The simulations were conducted for the 10 mm particle systems beyond the initial shearing process, observing the behavior until shearing was completely terminated.

The results from these simulations (blue), along with the experimental data (orange), are presented in Figure 7, Figure 8 and Figure 9. These figures compare the shear stress curves for the first shearing cycle for both 10 mm and 6 mm particle systems. For the qualitative comparisons within each figure, a single representative curve from each experimental series is shown (the curve chosen from each experiment has both the pre-shear and relaxation phases).

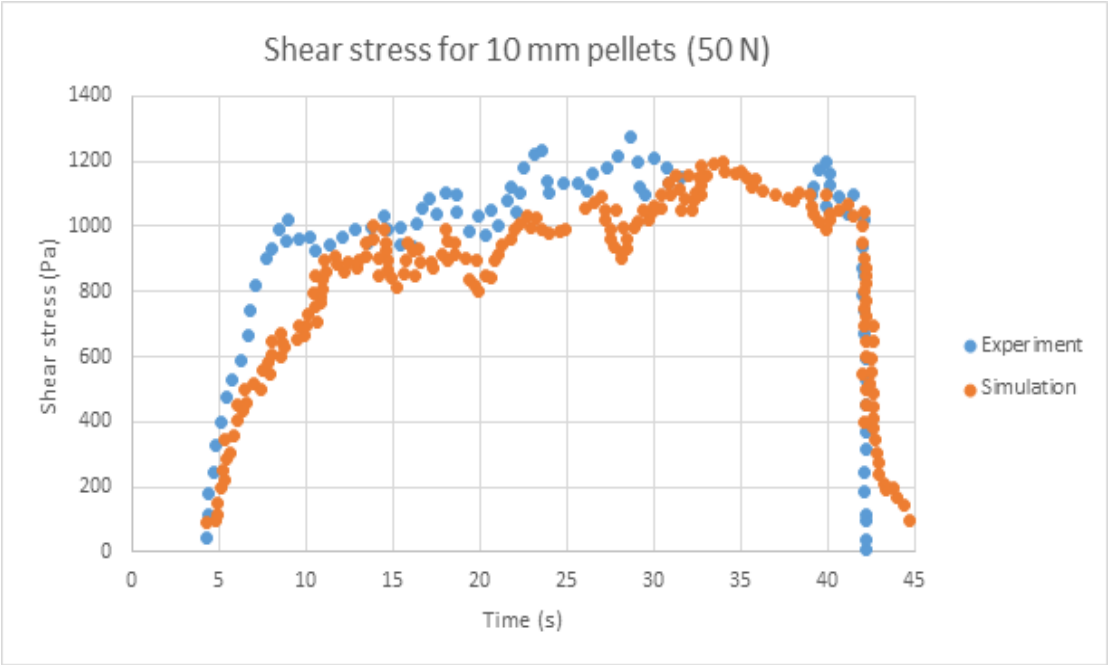

Figure 7: Shear stress curves during the first shear in the simulations (orange) and the experiments (blue) at a consolidation load of 50 N

Figure 7 presents the shearing curves obtained from simulations and experiments subjected to a normal force of 50 N. Similar qualitative trends are observed for the shearing curves acquired at a normal load of 25 N (Figure 8).

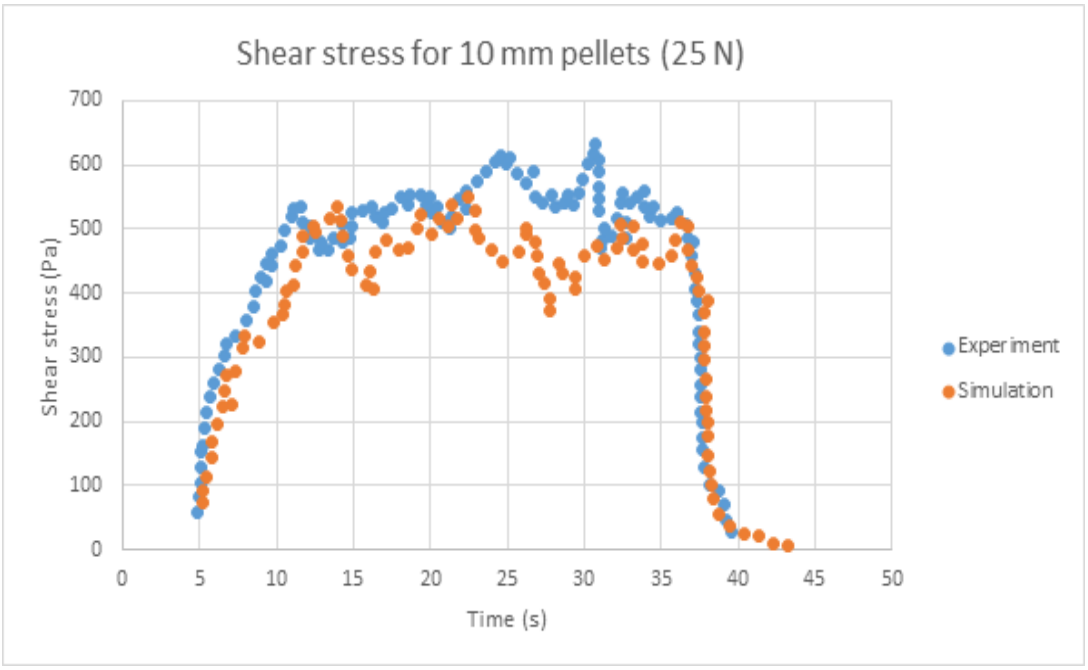

Figure 8: Shear stress curves during the first shear in the simulations (orange) and the experiments (blue) at a consolidation load of 25 N

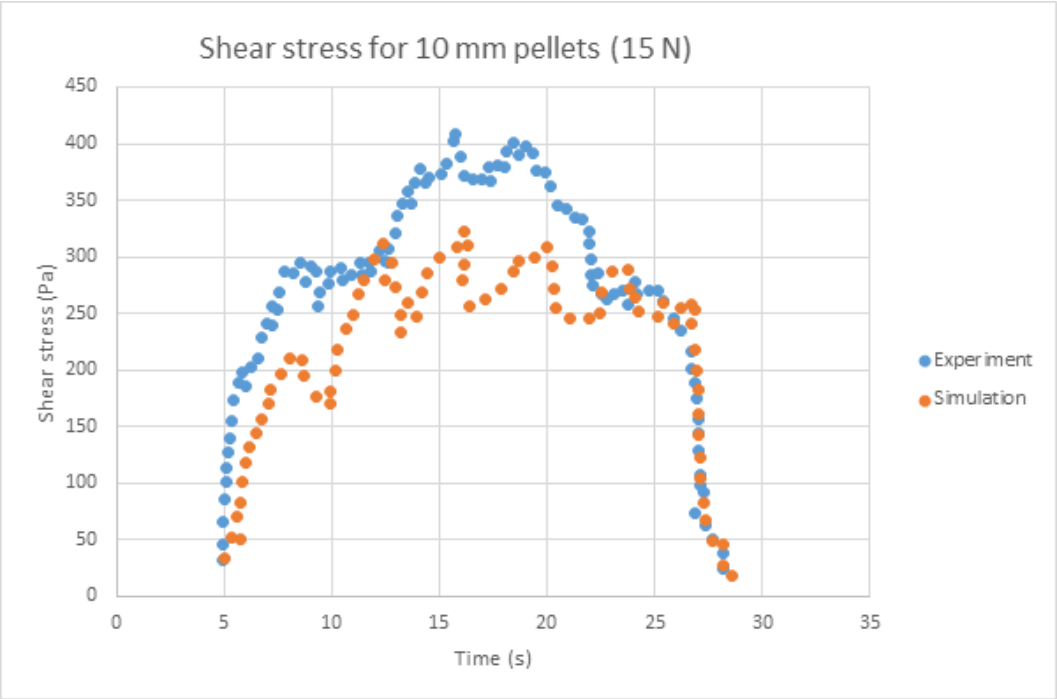

Figure 9: Shear stress curves during the first shear in the simulations (orange) and the experiments (red) at a consolidation load of 15 N

Cohesion model

During the reduction process, both the composition and the topological nature of iron ore continuously change. As a result, the adhesive forces within the bed also vary significantly. The altered particle shape, in particular, has a large influence on the mechanical interlocking within the bed. As the reduction progresses, the size of the objects continuously decreases, and edges and protruding corners are largely rounded off by melting processes and oxidation. This results in less pronounced material interlocking and consequently a significant decrease in adhesive forces between the objects.

To account for this effect in calculations, the cohesive force is individually described depending on the residual carbon content of each object. A model is needed that approximates both the physically inhomogeneous character and the motion behavior typical of iron ores, both qualitatively and quantitatively. To model these interlocking and adhesion effects, an extended force model based on the work of Luding et al. [7] is used. In this model, additional cohesive forces are imposed on a contact pair, so that additional energy (in the form of tensile force in the opposite direction) must be expended to separate the particle contact. Both the loading and unloading phases of a particle contact are described by a linear relationship between the normal force F and the virtual overlap δ using three different spring stiffnesses k_1, k_2, and k_c (Figure 10).

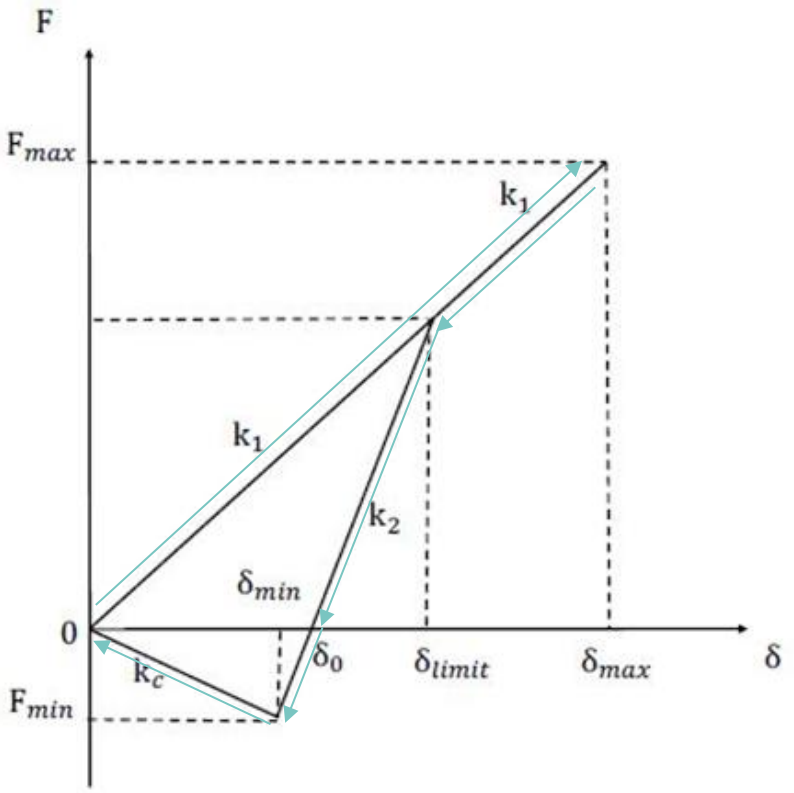

Figure 10: Extended Cohesion Model

When two objects are in contact, a virtual overlap occurs, and a spring is linearly loaded with stiffness 1. As soon as the particles move away from each other, the virtual overlap decreases, and the spring is initially unloaded again with spring stiffness 1. When the limit value δ_{limit} is undershot, the spring is instead unloaded linearly with spring stiffness 2. At the point where the force component becomes negative ($\delta<\delta_0$), the particles begin to adhere to each other, and the force becomes negative. If sufficient separation energy is applied, the particles move further apart, and from an overlap of δ_{min}, the spring is relaxed with stiffness c until there is no more overlap. From this point on, no adhesion forces act, and the contact is resolved. δ_{limit} thus directly limits the maximum mechanical work required to separate a contact pair. This corresponds to the area enclosed below the abscissa by k2 and kc.

This is particularly advantageous for very soft particles in contact, where a relatively large virtual overlap results. Without limiting the separation energy, extremely high cohesive forces would act on these contacts, making them difficult to break apart through mechanical actions. If, however, the kinetic energy applied to the contact is insufficient to exceed δ_{limit}, the maximum overlap of this contact is used as the reference value and directly relieved with the spring stiffness 2. Except for the spring stiffness 1, the other two spring stiffnesses 2 and c are determined empirically and specified as ratios to 1. For a suitable choice of parameter ratios regarding the average particle age and its variance on a moving grate, reference is made to a sensitivity analysis found in the works of Brosch [8]. Further approaches to modeling adhesive forces can be found in Kuwagi et al. [9] and in the review by Li et al. [10].

Experiments to simulate cohesion phenomena between particles were conducted at UNISA. A commercial grease (VIKY grease 51c) was mixed with wooden spheres to create a thin layer of adhesive material on the particle surface, promoting cohesion among them (Figure 11). Wooden spheres with a 6 mm diameter were selected, as their experimental results can be more easily interpreted using standard characterization procedures compared to larger particles.

Figure 11: Wood Particles with & without Grease

Cohesion was induced by coating the spheres with a thin layer of commercial silicon grease. This grease acts as a sliding agent, anti-seizing, and antioxidant material, and is insoluble in water. It complies with pharmaceutical standards (DAB, BP, USP, PE) and FDA regulations, with a working temperature range from -25°C to +100°C. After determining the required mass of particles for the sample, the amount of grease needed to form a 0.5 mm layer was calculated and added. The mixing process was carried out using a Wab tubular mixer to ensure uniform coating of the particles (Figure 12).

Figure 12: Wab Tubular Mixer Device

A visualization comparison is shown between the experimental and simulated images taken before and after applying the normal load.

1. Pre-Load Visualization

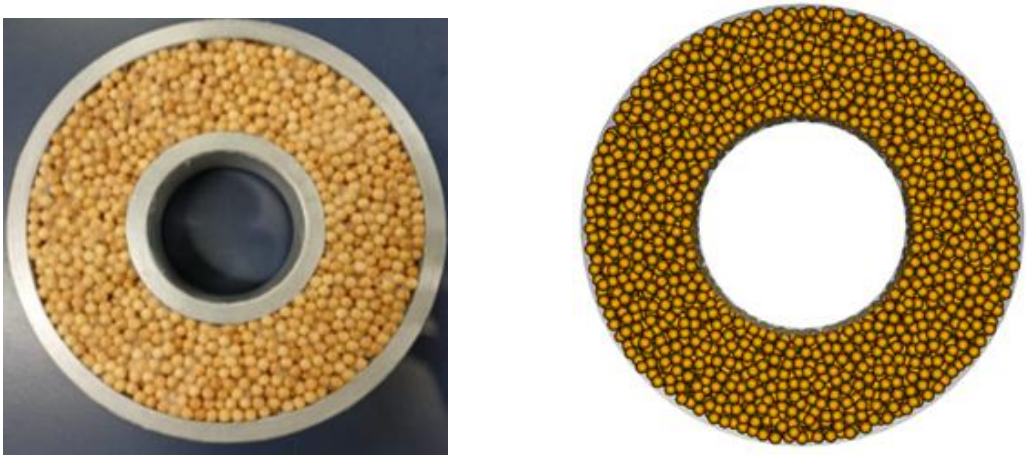

Figure 13: Pre-Load Experiment & Simulation Visualization

2. Post-Load Visualization

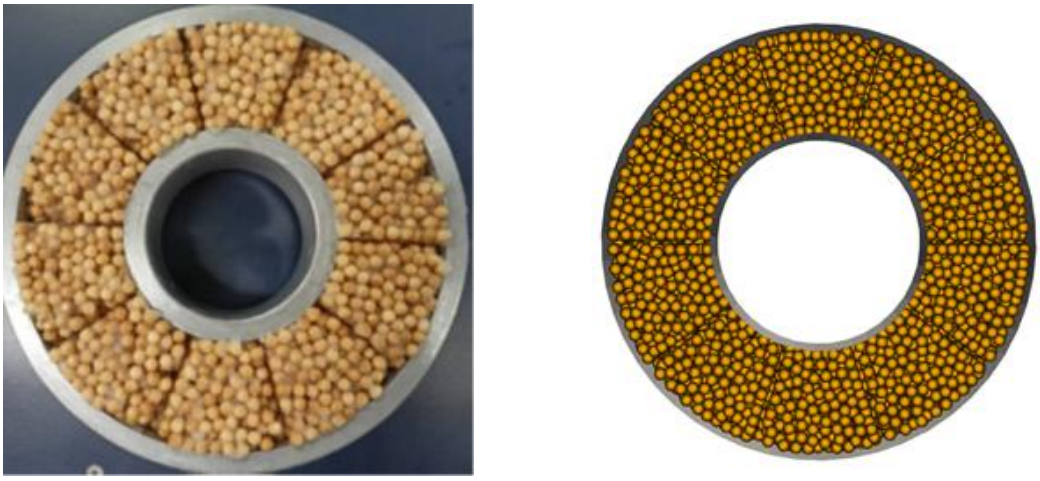

Figure 14: Post-Load Experiment & Simulation Visualization

Comparative analysis between the simulations with and without cohesion

A comparative study is conducted between the model with cohesion and the model without cohesion to understand the differences in particle behavior.

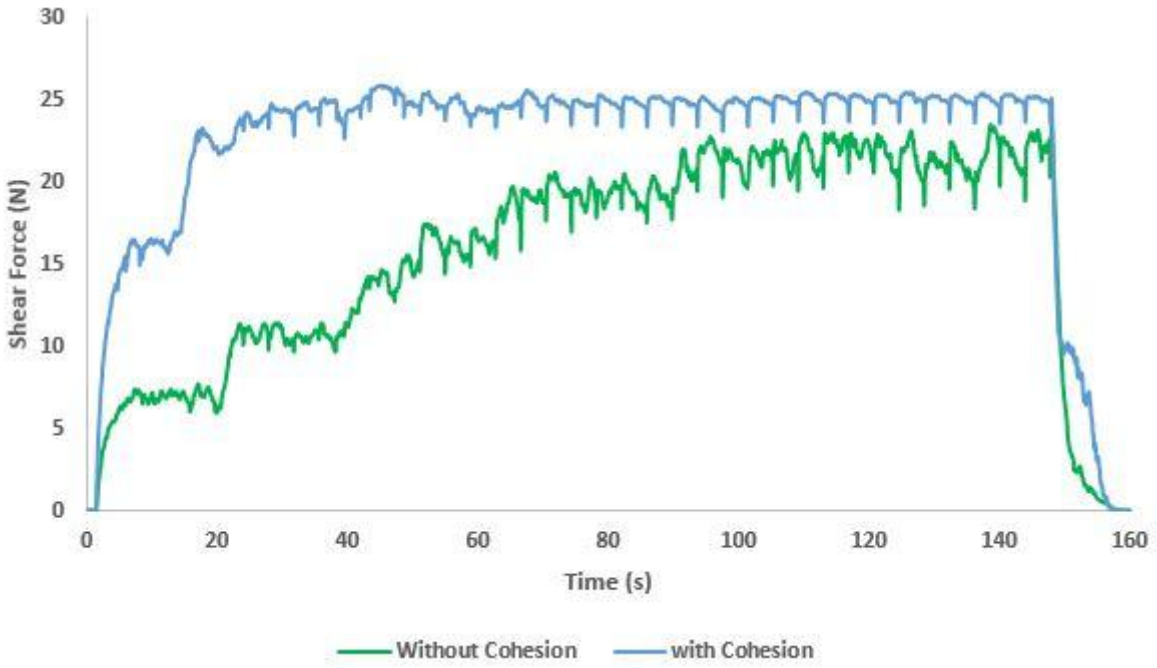

Figure 15: Shear force comparison for two simulation scenarios: with and without cohesion

The analysis reveals that in the absence of cohesion (see Figure 15), particles produce less shear force compared to the shear force produced when cohesion is implemented. The cohesion model results in reduced particle vibrations, providing smoother and more stable behavior. This difference highlights the role of cohesion in mitigating particle movement, preventing excessive fluctuations, and promoting more consistent interactions. By reducing the vibrations, the cohesion model enhances the accuracy and realism of the simulation, making it more aligned with observed experimental behavior.

Validation between simulation and experiments

After conducting a comparative study of different cohesion levels by adjusting the δ_{limit} parameter, the best simulation results were compared with experimental data to assess accuracy and reliability. Additionally, the comparison between simulations with and without cohesion highlights the differences in the model and demonstrates how cohesion successfully reduces particle vibration.

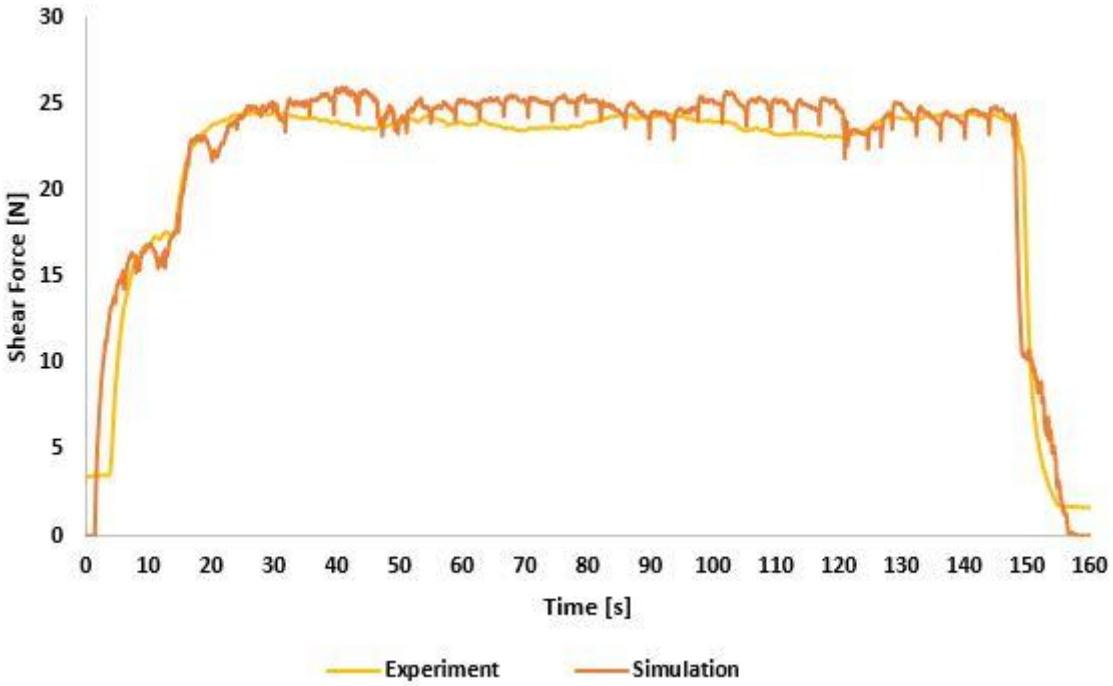

Figure 16: Experimental results at UNISA compared to simulation results from RUB

Figure 16 above validates the simulation results, showing good agreement with the experimental data. However, the simulations slightly overestimate the values at specific time intervals. While the overall behavior of the simulation closely mirrors the experimental results, the experiment shows a smoother curve with minimal vibration. In contrast, the simulation exhibits slight dips, which may be attributed to the Luding cohesion model.

This observation suggests potential future work, such as exploring alternative cohesion models to further reduce particle vibrations. Nevertheless, the Luding model effectively reduces the vibrations compared to simulations without cohesion, though it does not entirely match the smooth behavior observed in the experimental results.

2.3. Integration of the kinetic model in DEM/CFD code (RUB)

The reduction model from UL [11] has been implemented into the existing DEM code at RUB. The first set of results is shown in Figure 17. While the initial conversion has been completed, further work is required to achieve full integration. Specifically, the next phase involves coupling the CFD (Computational Fluid Dynamics) system with our existing codebase. Complete implementation of the model is planned for the end of the year and the first results will be included in the upcoming deliverable of WP2.

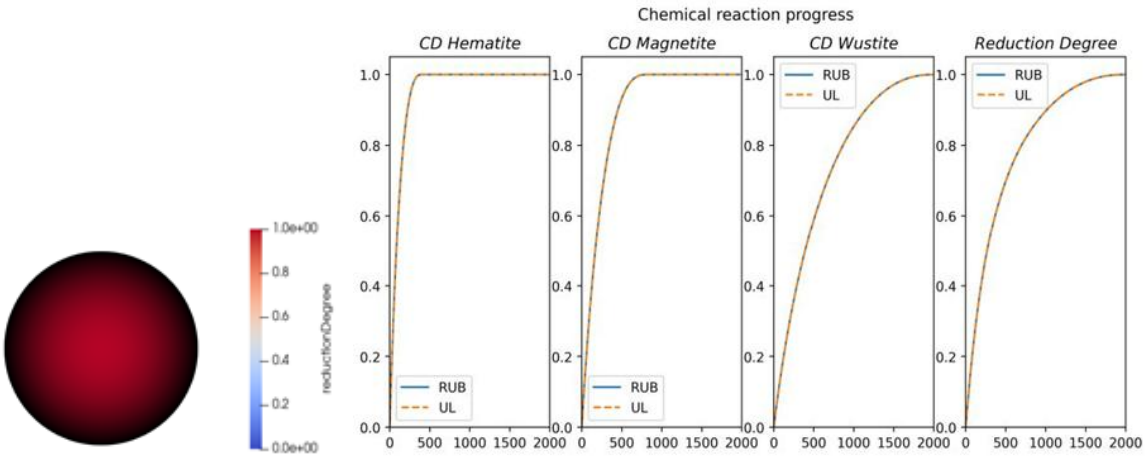

Figure 17: Comparison of the results from the kinetic model of UL with the RUB model describing the H_2 reduction of a single pellet at 900 °C for 2000 seconds

In the second test case, the simulation was scaled up to 200 particles. The goal here was to assess the behavior of the system with a higher number of particles interacting together. The starting test case was taken from the experiments conducted by Tata Steel with a simple vertical reactor [12].

A series of reduction experiments was conducted by TS and described in Deliverable 1.1 to investigate the behavior of direct reduction (DR) grade iron ore pellets in a hydrogen-enriched atmosphere. The gas composition used for the experiments consisted of 55% hydrogen (H_2) mixed with inert nitrogen gas. The experimental setup featured a reactor with an internal diameter of 69 mm (Figure 18), housing a sample bed approximately 75 mm in height. Gas was introduced into the system from the top through an 8 mm diameter inlet tube, with the outlet pressure maintained at atmospheric conditions to preserve a steady-state gas flow.

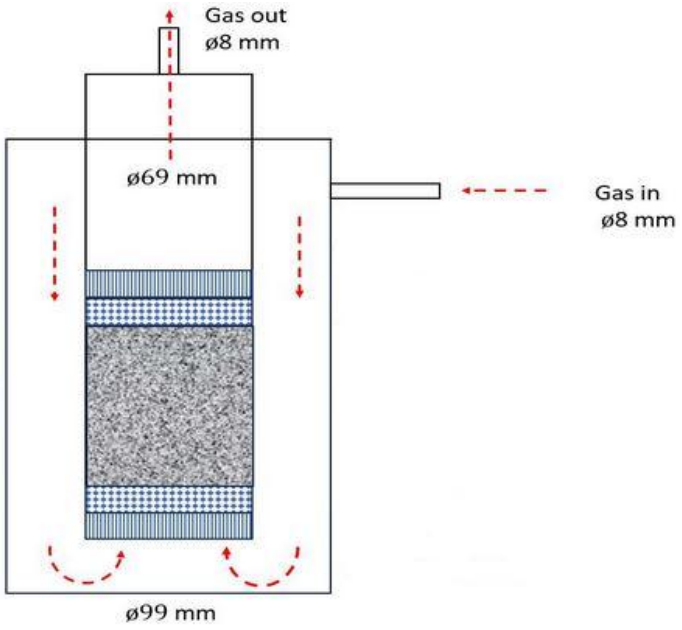

Figure 18: Sketch of the reactor used by Tata Steel for the experiments

The furnace used in the experiments ensured a homogeneous temperature distribution across the pellet bed, both in the axial and radial directions, allowing for uniform heating of the sample. The pellet bed consisted of DR-grade pellets, screened to a size range of 10–13 mm. While the precise bed porosity was not measured, this range aligns with typical values for DR-grade pellets under similar conditions. The sample mass used for each experiment was standardized at 500 grams,

and the reduction process was monitored through mass loss measurements, which were recorded for two different pellet types, labeled A1 and D1, to assess the kinetics and extent of reduction under the specified conditions.

The retort design included perforated plates at the top and bottom to support the sample and ensure uniform gas distribution. Layers of 13 mm aluminum oxide balls were placed above and below the pellet bed, contributing to consistent gas flow and thermal management within the setup.

Figure 19 below illustrates the first coupled DEM/CFD simulation. In this simulation, particle behavior (including contact interactions and reduction reactions) is modeled using the in-house DEM code developed at RUB, while the ambient conditions (such as gas flow, temperature distribution, and chemical species concentration) are computed through the CFD domain. The reduction degree of each pellet is dynamically calculated based on the local conditions, which are influenced by gas-solid interactions.

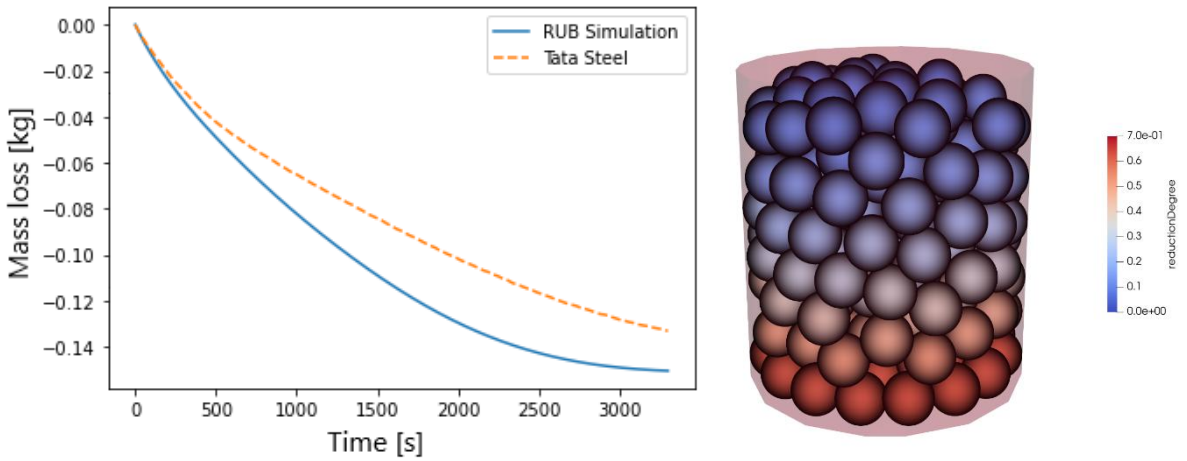

Figure 19: The first coupled DEM/CFD simulation using the reduction model from RUB. Mass loss is shown for 55 min. The reduction degree is shown for the temperature of 900 °C after 10 min.

On the left, the graph depicts mass loss over 3,300 seconds (55 minutes), with the RUB simulation (solid blue line) showing a steeper decline than the TS experiment (dashed orange line). This discrepancy may be attributed to differences in material properties, particularly particle size. The TS experiment uses particles ranging from 10–13 mm, whereas the simulation assumes monodisperse particles (12 mm). The visualization on the right side shows the pellets within the packed bed, with color gradients representing the reduction degree for each individual pellet. All other boundary conditions match those of the TS experiment, as described previously.

2.4. Integration of the sub-models in Reductor model (UL)

The single pellet kinetic model has been successfully implemented in the Reductor model.

The integration of an analytical code in a 2D Finite Volume Method (FVM) mesh was performed as follows:

- Each physical parameter that could vary within the furnace was indexed and associated with a specific cell (i,j) of the furnace mesh. For example, molecular masses did not require an index, but reaction rates did: $r_1 \rightarrow r_1(i,j)$.
- Unlike a thermobalance setup, the shaft furnace operates under non-isothermal conditions with variable gas composition. Therefore, it was necessary to find a way to adapt the kinetics to describe reduction processes under varying external conditions surrounding the pellet.

Following the work of Sohn [13], we adapted the law of additive reaction times in differential form for each sub-reaction, as shown below:

$$r_X = \frac{1}{\sum_k \tau_k \cdot f_k(X)}$$

Where the denominator is the sum of characteristic times multiplied by conversion functions, and each one of these is related to a phenomenon that could be rate-limiting in the reaction, such as mass transfer of reducing gas, diffusion of gas through the pellets pores, and local chemical reaction. This law has proven effective in describing reduction kinetics under varying bulk gas and temperature conditions [14].

- Given the variability in gas composition, we implemented two gas-gas reactions: methane steam reforming and the water-gas shift reaction, respectively listed below:

$$CH_4 + H_2O = CO + 3H_2$$
$$CO + H_2O = CO_2 + H_2$$

- Another fundamental difference with the thermobalance situation is the steady-state operation of the shaft furnace. Mathematically, the conversion of pellets progresses not with time, but as they descend through the furnace.
- Finally, the pellet bed is modeled as a flow of individual pellets with a constant bed porosity of 0.5.

With these considerations, we derived the transport equations for each species involved in the reduction process. We give a schematic example of the discretized equation for the mass fraction of magnetite in the solid burden in an arbitrary cell (i,j):

$$a(i,j) \cdot \omega_{Fe_3O_4}(i,j) = \sum_N a_N \cdot \omega_{Fe_3O_4,N} + V_C(i,j) \cdot MM_{Fe_3O_4} \cdot \sum_k \nu_{Fe_3O_4,k} \cdot \rho^*_{Fe_xO_y,k,ini}(i,j) \cdot r_k(i,j)$$

Where the transport coefficients labeled *a(i,j)* and a_N are related to the solid movement; the index N denotes the neighboring cells of (i,j), such as (i+1,j), (i,j-1), etc. V_C is the cell volume and $MM_{Fe_3O_4}$ is the molecular weight of magnetite. The ν coefficients are the stoichiometric coefficients of magnetite in the different reactions it is involved in; $\rho^*_{Fe_xO_y,k,ini}$ represents the equivalent quantity of oxide introduced in the burden for the reduction reaction; finally, the bed porosity is embedded within $\rho^*_{Fe_3O_4,ini}$ and in the reaction rates r_k.

In the code, multiple subroutines solve the various transport equations. One subroutine determines the reaction rates in each cell depending on the local conditions (temperature, gas composition, solid conversion); these reaction rates are then utilized in the transport equations for both solid and gas species, ensuring proper mass balance of species. The same principle is applied to the heat transport equations.

2.5. Integration of the sub-models in FEM shaft model (BFI)

The UL grain reduction kinetics sub-model is implemented into the BFI multiparticle FEM reactor model. The BFI model is built using the COMSOL Multiphysics. The gas flow through the packed bed is modelled using the Brinkman Equations. The solid particle flow is predefined, but it will be approximated by a rheology model. The packed-bed and gas temperature fields are modelled separately considering the heat exchange in-between them as well as reaction heats. The transports of the solid and gas species are modelled, too. The chemical reactions are modelled using the chemistry interface. The screenshots of all these interfaces are briefly shown in Figure 20 below.

The BFI FEM model uses a thermo-dynamical package to describe the gas mixture properties (e.g., density, enthalpy, entropy, heat capacity, heat capacity ratio, diffusivity, thermal conductivity, and viscosity). The system uses the ideal gas (available other options are Peng-Robinson, Peng-Robinson-Twu, Soave-Redlich-Kwong, Soave-Redlich-Kwong-Graboski-Daubert), the thermal conductivity is estimated using the kinetic theory (available other options is ideal), and gas viscosity is estimated by Wilke model (available other options are Brokaw, Davidson, Wilke-high-pressure, Brokaw-high-pressure, Davidson-high-pressure, Pedersen). The mixture components or underlying sub-models can be changed easily. The needed other variables of the UL model are defined as they appeared in the UL-python-code.

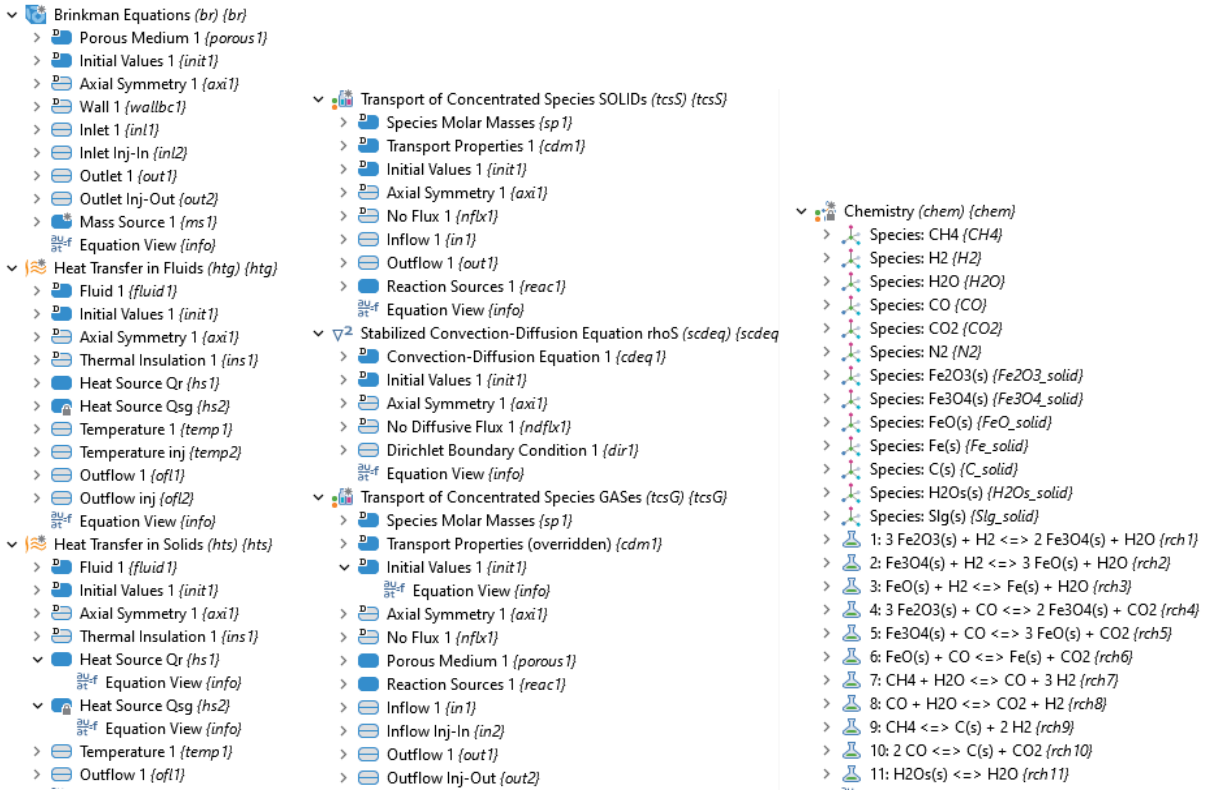

Figure 20: screenshots showing the physics interfaces used in BFI FEM model.

Comparison of the reduction curves (i.e., the evolution of weight fractions of solid species) of 14 mm sized pellets in 30% H_2, 30% CO, 40% N_2 atmosphere at 1 atm and 900 °C is performed. The results obtained from the UL-python script are shown on the left side, the results obtained by the BFI FEM implementation are shown on the right side in Figure 21. The same simulations in Figure 1 for the temperature dependency of the reduction are reproduced with the BFI-FEM implementation. A comparison of these results is given in Figure 22. The small differences are probably due to the different diffusivities (which is induced mostly by the choice of inert gas as N_2 instead of He, the usage of COMSOL Multiphysics® built-in thermodynamical database might also have the same effects).

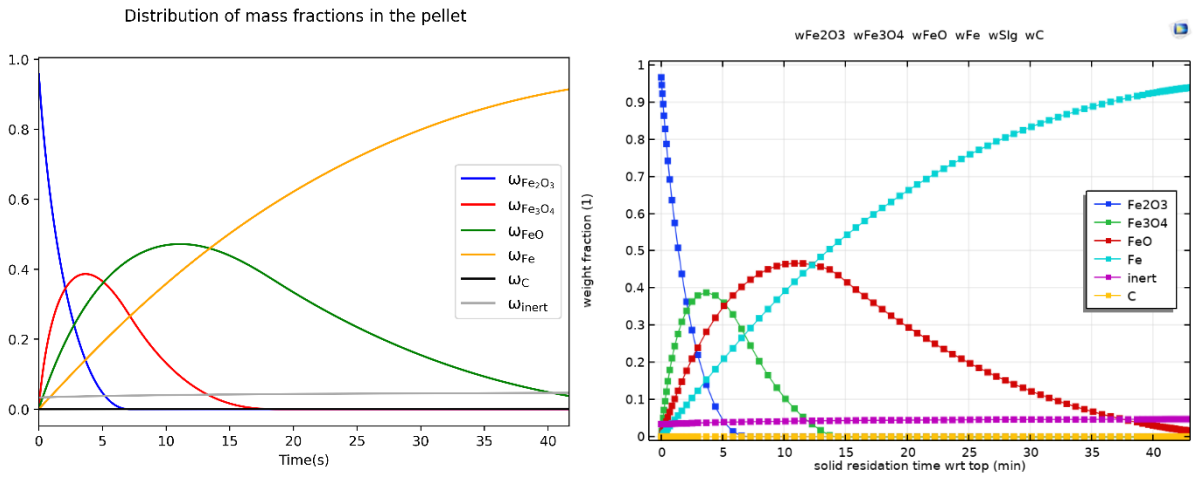

Figure 21: Comparison of reduction curves of 14 mm sized pellets in 30% H_2, 30% CO, 40% N_2 atmosphere at 1 atm and 900 °C. (left: UL-python script, right: BFI FEM implementation)

Comparison of the reduction curves for various isothermal cases for 15mm sized pellets in 55% H_2 and 45% N_2 atmosphere at 1 atm. The results obtained from UL are shown on the left side, the results obtained by the BFI FEM implementation are shown on the right side in Figure 22. The small differences are due to different thermodynamic databases (which induce, e.g., small differences in the diffusivities, etc.).

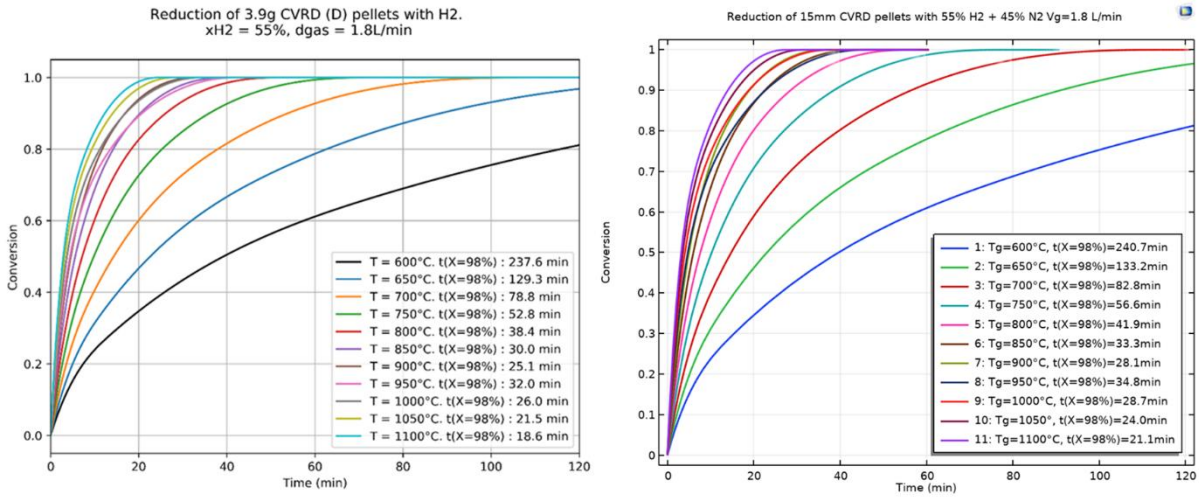

Figure 22: Comparison of reduction curves of 15 mm sized CVRD pellets in 55% H_2, 45% N_2 atmosphere at 1 atm and various isothermal temperatures.
(left: UL-python script, right: BFI FEM implementation)

As shown in Figure 23a on the left side, the experimental reduction curves provided by TSE Ijmuiden can be reproduced by the BFI-FEM model with the original kinetic triplets $(k_{0,i}, Ea_i)$. As UL suggested, the kinetic triplets can be optimised for a better fit of model to experimental observations. The reduction degree of pellets at t=10 minutes is plotted on the right side of Figure 23b, which is very similar to the DEM/CFD results of RUB given in

Figure 19.

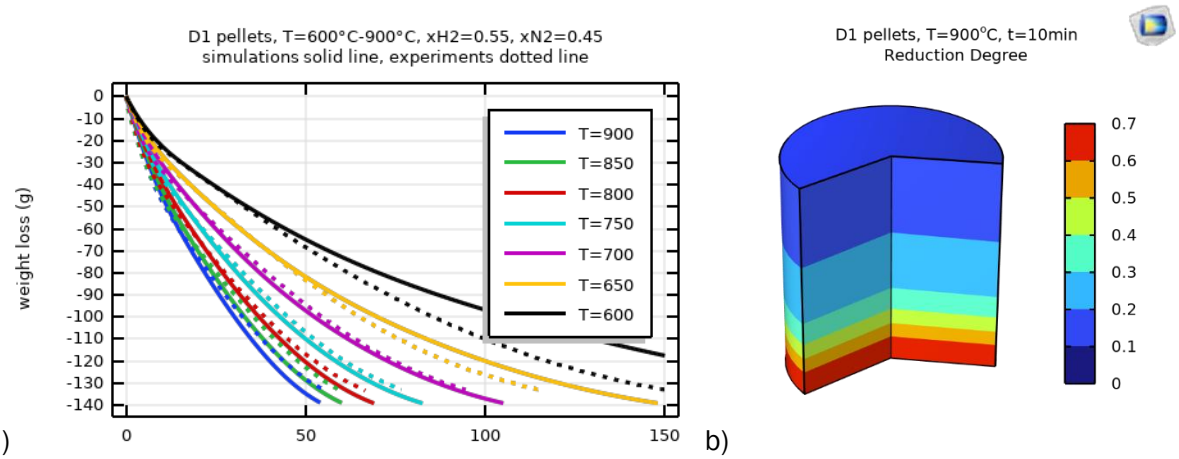

a) b)

Figure 23: Comparison of TSE experimental reduction curves (dashed lines) and reduction curves obtained by BFI-FEM (solid line) for various temperatures.

3. Results

3.1. Reductor model

The Reductor model completed with the single pellet kinetic model allows the simulation of the working point of a shaft furnace operating under syngas or hydrogen conditions.

Simulation of a syngas-based shaft furnace

The operation under syngas conditions is derived from the Contrecoeur Midrex plant. It has previously been simulated and validated against plant data; it will serve as a reference case for future simulations. It includes both a bustle gas and a cooling gas circuit (inlet and outlet, see Figure 24). It operates at relatively low pressures (1.5-2 bar) and with a relatively low H_2 content in the gas (x_{H2}~50%).

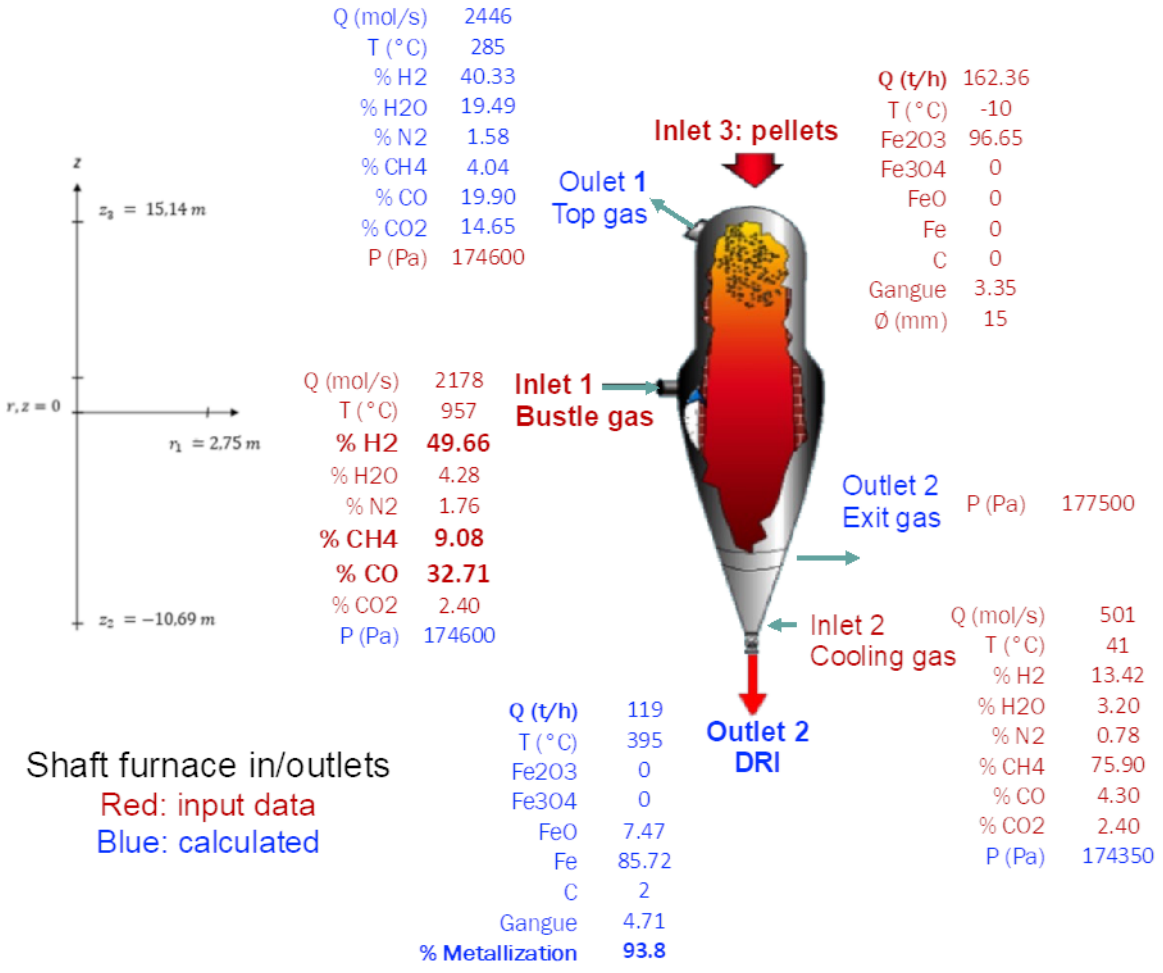

Figure 24: Working conditions of a syngas shaft furnace.

The simulation results are available in Figure 25. We see that the temperature decreases quickly near the bustle inlet; this is the same for H_2 and CO content, indicating that the bustle gas struggles to flow through the burden. Oxides conversion occurs over a large portion of the reduction zone,

and the metallization of the outer burden is completed 4 meters above the bustle inlet. However, the center zone of the furnace remains non-metallized, resulting in an overall metallization of 94%. Natural gas injected at the bottom of the shaft helps in cooling and carburizing the DRI in the hopper. Most of this gas is evacuated through the cooling gas outlet to prevent deterioration of the thermochemical conditions in the reduction zone. The reforming process slightly replenishes H_2 and CO contents right under the bustle inlet, but it also cools the furnace center (hence the light blue cylindrical zone in the furnace top center on the temperature map). Carbon deposition is most efficient directly under the bustle inlet, catalyzed by metallic iron through the reverse Boudouard reaction and the methane decomposition. In the furnace center, the non-metallized burden impedes carbon deposition. Complete simulation parameters and results are available in reference [15].

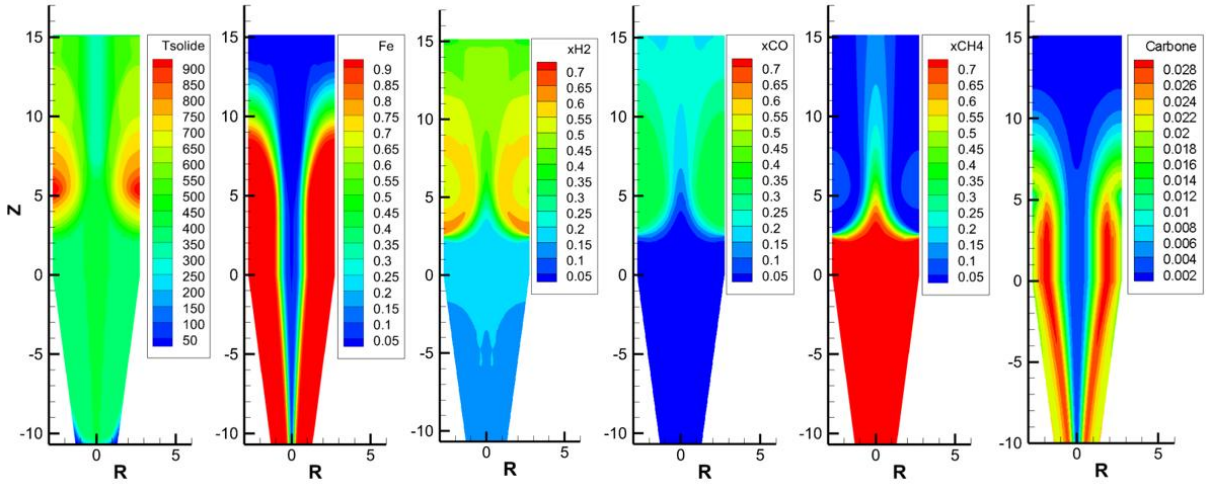

Figure 25: Simulation results for a syngas shaft furnace. From left to right; solid temperature; iron content; H_2 content; CO content; CH_4 content; carbon content.

Simulation of a hydrogen-based shaft furnace

Using the syngas shaft furnace as a reference case, we derived hypothetical conditions for the operation of a new hydrogen-enriched shaft furnace (see Figure 26).

The model and boundary conditions are similar to those of the syngas case (low pressure operation, same gas and solid flows at inlets) but it does not utilize a cooling gas outlet. The hydrogen that cools down the metallized burden then flows upwards in the reduction zone to replenish H_2 content in the gas. This allows to obtain full metallization of the burden and prevent hydrogen depletion in the furnace centre. The temperature at the bustle is set slightly lower (850 °C) to demonstrate that full metallization is feasible with high H_2 content at relatively moderate temperatures.

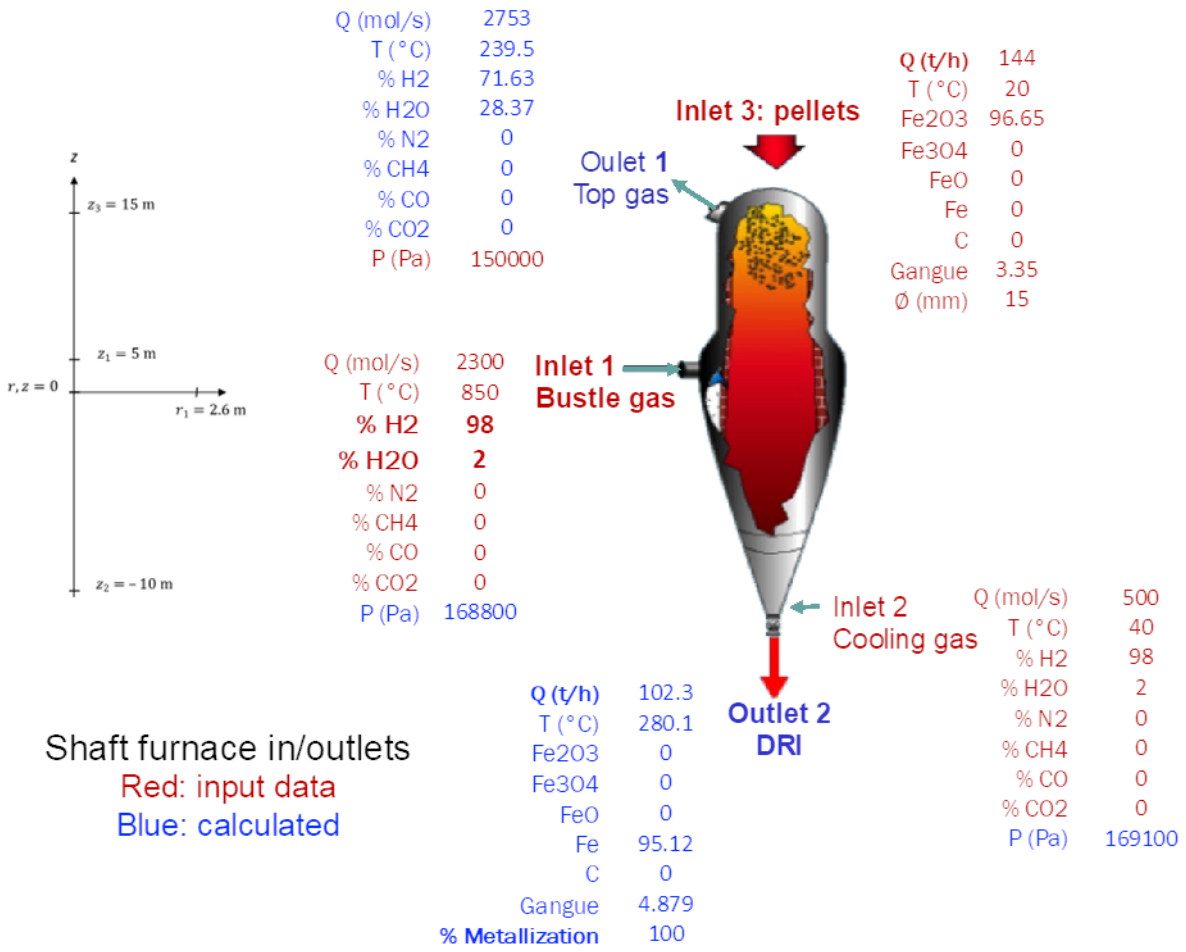

Figure 26: Working conditions of a hypothetical H_2 shaft furnace.

Specific results are shown in Figure 27: we see that conversion occurs throughout the entire height of the reduction zone, indicating an efficient shaft operation.

However, at a given radius, the conversion takes place over a small vertical area compared to the syngas operation, primarily due to the faster reduction kinetics with H_2 than with H_2+CO. Nevertheless, solid temperature and H_2 content increase rapidly within the first 3 meters from the furnace top, leading to a quick metallization near the furnace wall.

These two representative simulations were selected among others carried out by UL with the new SPKM. It was also found that the behavior of the furnace changes according to the gas-to-solid flowrate ratio, as presented in the last two General Assemblies. These results are not reported here, being out of the scope of the present deliverable.

Further simulations will explore varying gas bustle properties, particularly temperature and gas composition, to determine how inlet parameters affect performance indicators such as energy consumption and gas utilization efficiency. This paves the way towards WP2, in which the operation of the 100% H_2 shaft furnace will be studied in greater detail.

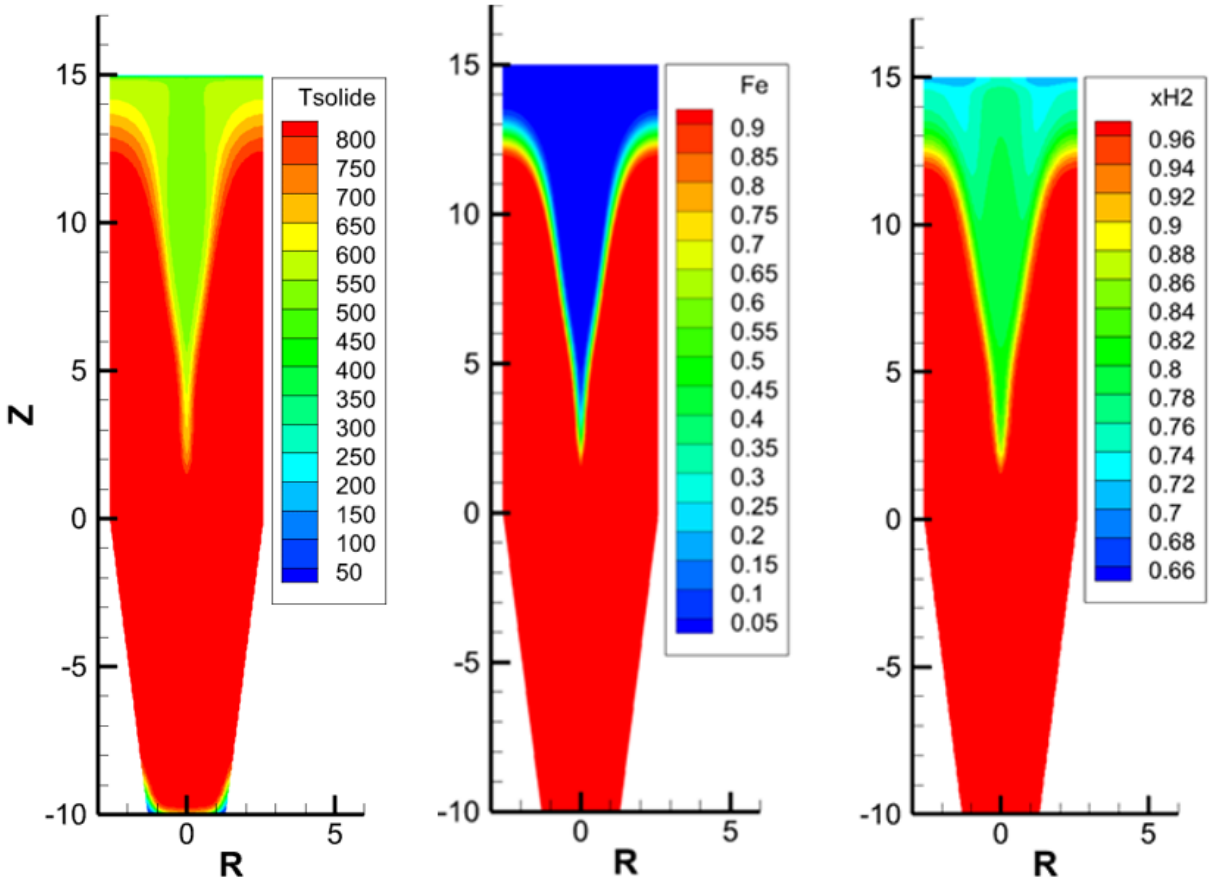

Figure 27: Simulation results for a hydrogen shaft furnace. From left to right: solid temperature, iron content, and H_2 content in the furnace.

4. Conclusion

This deliverable presents the collaborative efforts and progress achieved by UL, RUB, and BFI in Task 1.4, focusing on the integration of new kinetic sub-models into direct reduction (DR) shaft process models. Each partner has made significant contributions toward the implementation and validation of the single pellet kinetic model (SPKM) within their respective modelling frameworks.

RUB has advanced in integrating the SPKM into their discrete element method/computational fluid dynamics (DEM/CFD) code. Preliminary shear cell simulations have been conducted to validate mechanical interaction parameters, and efforts are underway to implement a cohesion model that accounts for adhesive forces between particles under DR conditions. Full integration of the kinetic model into the DEM/CFD code is anticipated by the end of the year, which will enhance the understanding of particle-level interactions in the DR process.

BFI has successfully implemented the SPKM into their finite element method (FEM) shaft model using COMSOL Multiphysics. Their model effectively simulates gas flow, solid particle flow, temperature fields, and chemical reactions within the DR shaft furnace. The integration shows excellent agreement with UL's original model, validating both the accuracy and reliability of the FEM reactor model and contributing to more accurate predictions of chemical transformations and metallization degrees.

UL has successfully integrated the SPKM into their Reductor model, enabling the simulation of both syngas and hydrogen-based shaft furnaces. Their simulations demonstrate promising results, including optimized shaft operations and full metallization under hydrogen-rich conditions, laying a foundation for further exploration in hydrogen-enriched DR technologies.

The combined efforts of UL, RUB, and BFI ensure compatibility of results across different modelling approaches — finite volume, DEM/CFD, and FEM — providing a comprehensive understanding of the DR process. These advancements establish a robust foundation for the simulations planned in Work Package 2 (WP2), where these enhanced models will be utilized to study the DR process in greater depth.

5. References

(in order of appearance in the text)

[1] J. Jägers, M. Brömmer, E. Illana, S. Wirtz, V. Scherer, DEM-CFD simulation of wood pellet degradation by particle-wall impact during pneumatic conveying, Powder Technology, Volume 391, 2021, 385-402, ISSN 0032-5910, https://doi.org/10.1016/j.powtec.2021.06.037.

[2] Michael Oevermann, Stephan Gerber, Frank Behrendt, Euler–Lagrange/DEM simulation of wood gasification in a bubbling fluidized bed reactor, Particuology, Volume 7, Issue 4, 2009, 307-316, ISSN 1674-2001, https://doi.org/10.1016/j.partic.2009.04.004.

[3] S. Bollmus. Biologische und technologische Eigenschaften von Buchenholz nach einer Modifizierung mit 1,3-dimethylol-4,5-dihydroxyethyleneurea (DMDHEU), Göttingen: *Cuviller Verlag, 2011.*

[4] P. A. Cundall and O. D. L. Strack. A discrete numerical model for granular assemblies. *Géotechnique, pp. 47 65, 1979.*

[5] B. Blais, D. Vidal, F. Bertrand, G. S. Patience and J. Chaouki. Experimental Methods in Chemical Engineering: Discrete Element Method DEM. *The Canadian Journal of Chemical Engineering, pp. 1964 1973, 2019*.

[6] J. Schäfer, S. Dippel und D. Wolf. Force Schemes in Simulations of Granular Materials. *Journal de Physique I, pp. 5-20, 1996.*

[7] S. Luding, K. Manetsberger, J. Müllers: A discrete model for long time sintering. *Journal of the Mechanics and Physics of Solids 2005, 53:455–91.*

[8] B. Brosch, S. Wirtz, V. Scherer: A particle-based model for the combustion of municipal waste in grate firing systems. *9th European Conference on Industrial Furnaces and Boilers, Estoril, 2011.*

[9] K. Kuwagi, T. Takami, A. Bin Alias, D. Rong, H. Takeda, S. Yanase, et al.: Development of DEM-CFD simulation of combustion flow in incinerator with the representative particle model. *Journal of Chemical Engineering of Japan 2016, 49:425–34.*

[10] S. Li, J.S. Marshall, G. Liu, Q. Yao: Adhesive particulate flow: The discrete-element method and its application in energy and environmental engineering. *Progress in Energy and Combustion Science 2011, 37:633–68.*

[11] A. Ranzani da Costa, D. Wagner, F. Patisson, Modelling a new, low CO2 emission, hydrogen steelmaking process. *Journal of Cleaner Production, Volume 46, 2013: 27-35, ISSN 0959-6526, https://doi.org/10.1016/j.jclepro.2012.07.045.*

[12] J. Small, C. Buytendijk, M. Ntouma, Y. Xiao, E. Zinngrebe, C. Kooij, S. Melzer, M. van Wijngaarden, F. van der Does, S. van der Laan. Isolating the influence of mineralogy and microstructure on iron-ore sinter reduction in the shaft and reserve zones of the blast furnace: lab experiments and thermodynamic modelling. *ECIC-ICSTI 2022*

[13] H. Y. Sohn (1978). The Law of Additive Reaction Times in Fluid-Solid Reactions. *Metallurgical Transactions B, vol 9B, 89-96*

[14] Patisson, B. Dussoubs, and D. Ablitzer “Using Sohn’s law of additive reaction times for modeling a multiparticle reactor. The case of the moving bed furnace converting uranium trioxide into tetrafluoride”, Sohn International Symposium “Advanced processing of metals and materials”, 27-31 Aug. 06, San Diego. Proceedings edited by F. Kongoli and R.G. Reddy, TMS, vol. 1 “Thermo and physicochemical principles: non-ferrous high-temperature processing”, 141-153.
<http://hal.archives-ouvertes.fr/hal- 00265646/fr~

[15] H. Hamadeh, O. Mirgaux, F. Patisson (2018). Detailed Modeling of the Direct Reduction of Iron Ore in a Shaft Furnace. *Materials*, 11,1865. http://dx.doi.org/10.3390/ma11101865